

# Lubricant-Infused Polymeric Interfaces: A Stretchable and Anti-Fouling Surface for Implantable Biomaterials

Tae Young Kim, Soohwan An, Young Kim, Seung Yeop Han, Jeuhee Lee, Kijun Park, Sangin Kim, Jae Park, Soo A Kim, Justin J. Chung, Seung-Woo Cho, and Jungmok Seo\*

Developing thin, highly stretchable coatings that inhibit the undesirable adhesion of biological substances on soft and high-water-content biomaterial surfaces is an area of significant interest. In this study, a stretchable antifouling coating named lubricant-infused poly(1,3,5,7-tetramethyl-1,3,5,7-tetravinyl cyclotetrasiloxane) (V4D4) is introduced interface with perfluoropolymer (L-VIP). The stretchable adhesive-perfluoropolymer bilayer comprises stretchable adhesive polymer (V4D4) and perfluoropolymer (1H,1H,2H,2H-perfluorooctyl methacrylate (FOMA)). The bilayer exhibits a strong affinity with the lubricant, imparting exceptional antifouling and slippery properties. L-VIP coating displays superior fouling resistance against plasma proteins related to foreign body reactions (FBR) and biofilm-forming bacteria. The coating exhibits impressive elastic limits exceeding 200% strain and exceptional stability under repeated cyclic stretching (> 2000 cycles at 150% strain) while maintaining its antifouling properties. Furthermore, the coating presents dielectric performance under accelerated aging conditions at a temperature of 70° and constant voltage stress of 10 V s<sup>-1</sup> for over 50 days. To assess the biocompatibility of the L-VIP coating, a series of in vitro and in vivo experiments are conducted, confirming its non-toxicity for biomedical applications. It is expected that the stretchable L-VIP coating will enhance medical devices' longevity and help prevent bacterial infections, the formation of biofilms, and the nonspecific adherence of biological substances after implantation.

## 1. Introduction

Implantable bioelectronic devices, such as cardiac pacemakers, glucose sensors, and electrocorticograms, have been widely adopted to monitor and treat chronic diseases by transmitting bioelectronic signals across human tissues.<sup>[1]</sup> However, once implanted, these devices are continuously subjected to external stresses due to breathing, blood circulation, muscle movements, and locomotion. Conventional bioelectronics is often made of mechanically robust materials with a high Young's modulus ( $\approx$ GPa) to withstand these stresses. Nevertheless, this mechanical mismatch with human tissues, which typically have a modulus in the range of 0.4 to 2000 kPa, can lead to adverse side effects, including tissue damage, inflammatory responses, and degeneration of surrounding tissues.<sup>[2,3]</sup> Recently, significant efforts have been made to develop soft bioelectronics that can seamlessly integrate with human tissues. Researchers have employed various biomaterials, fabrication strategies, and device designs using soft elastomers and water-rich hydrogels to develop soft bioelectronics with a modulus comparable

T. Y. Kim, J. Lee, K. Park, S. Kim, J. Park, S. A Kim, J. Seo  
 School of Electrical and Electronic Engineering  
 Yonsei University  
 50-1 Yonsei-ro, Seodaemun-gu, Seoul 03722, Republic of Korea  
 E-mail: [jungmok.seo@yonsei.ac.kr](mailto:jungmok.seo@yonsei.ac.kr)  
 S. An, S. Y. Han, S.-W. Cho  
 Department of Biotechnology  
 Yonsei University  
 50-1 Yonsei-ro, Seodaemun-gu, Seoul 03722, Republic of Korea  
 Y. Kim, J. J. Chung  
 Department of Transdisciplinary Medicine  
 Seoul National University Hospital  
 Seoul 03080, Republic of Korea

S. Y. Han  
 Department of Biomaterials Science and Engineering  
 Yonsei University  
 50-1 Yonsei-ro, Seodaemun-gu, Seoul 03722, Republic of Korea  
 J. Lee, J. Park, J. Seo  
 Lynk Solutec Inc  
 Yonsei University  
 50-1 Yonsei-ro, Seodaemun-gu, Seoul 03722, Republic of Korea  
 J. J. Chung  
 Department of Medicine  
 Seoul National University College of Medicine  
 Seoul 03080, Republic of Korea

 The ORCID identification number(s) for the author(s) of this article can be found under <https://doi.org/10.1002/adfm.202312740>

DOI: 10.1002/adfm.202312740

to that of human tissues.<sup>[4]</sup> Especially, hydrogel-based bioelectronics have been developed as next-generation interfaces due to their mechanical similarities to biological tissues and versatility in biofunctional, mechanical, and electrical engineering.<sup>[5,6]</sup>

In addition to the mechanical mismatch, the implantation of foreign materials can trigger immune-related side effects, also known as foreign body reactions (FBR). The FBR is initiated by the non-specific adhesion of biological substances (e.g., body fluid proteins, immune cells, and fibroblasts) onto bioelectronics, potentially causing FBR cascades and the formation of fibrotic encapsulation.<sup>[7]</sup> Moreover, foreign materials are susceptible to microbial infection and biofilm formation, leading to severe post-operative infections.<sup>[8,9]</sup> To minimize these side effects, patients often receive pharmacological treatments such as antibiotics and immunosuppressants.<sup>[10]</sup> Despite the effective elimination of infections and modulation of immune responses using these drugs, their frequent use is associated with antibiotic resistance and an increased risk of bacterial and yeast infections. In severe cases, patients may require reoperation to replace malfunctioning devices, potentially resulting in muscle paralysis, chronic pain, and life-threatening symptoms.<sup>[11,12]</sup>

Hydrophilic polymer-based anti-fouling coatings have been demonstrated to significantly reduce FBR and biofilm formation. Polymer brushes (e.g., poly(ethylene glycol) (PEG) based coatings) covalently attached to substrate surfaces exhibit exceptional fouling resistance properties by absorbing thin water layers.<sup>[13,14]</sup> However, certain limitations have been reported. Hydrophilic coatings sometimes may encounter challenges when applied to highly rough or irregular surfaces.<sup>[15]</sup> Furthermore, they are susceptible to mechanical wear and tear within dynamic *in vivo* settings, and their degradation can occur due to the presence of certain enzymes in the body, such as esterase, leading to a reduction in their anti-fouling capabilities.<sup>[16]</sup> In particular, the characteristics of polyethers place significant constraints on their enzymatic degradation.<sup>[17]</sup> Additionally, polymer brushes are susceptible to auto-oxidation under physiological conditions, potentially impeding their practical utility in clinical environments.<sup>[18]</sup>

Various approaches have been explored to increase the durability of anti-biofouling coatings in implantable medical devices.<sup>[19]</sup> As a promising solution, superhydrophobic surface modification has emerged. Superhydrophobic surfaces with low surface energy and hierarchical nano-microstructures offer anti-fouling properties by forming air pockets between the fouling liquids and substrate surfaces.<sup>[20,21]</sup> Hu et al. developed a stretchable and anti-fouling superhydrophobic coating for use in soft material devices, such as stretchable electronics, functional textiles, and flexible sensors.<sup>[22]</sup> The superhydrophobic coating was fabricated using a spraying method that combined polybutadiene (PB) and carbon black (CB) nanoparticles to create a highly deformable hierarchical structure. This coating offers advantages such as an easy fabrication process, mechanical stability, and high stretchability, capable of withstanding tensile strains. However, the thermal curing process at 120°C for 1 hour limits its application to soft bioelectronic materials, particularly high-water-content hydrogels. Recently, Oh et al. developed a stretchable and anti-fouling superhydrophobic coating by depositing a stacked polymer film consisting of poly(1,3,5-trivinyl-1,3,5-trimethylcyclotrisiloxane) (p(V3D3)) and poly(1H,1H,2H,2H-perfluoroctyl acrylate) (p(PFOA)) layers us-

ing initiated chemical vapor deposition (iCVD).<sup>[23]</sup> The resulting copolymer superhydrophobic film exhibited excellent fouling resistance against various chemical organic solvents and an elastic limit greater than 200% strain. However, the relatively long coating process (more than 1 h) makes it unsuitable for hydrogels. Beyond the time issue, concerns have arisen regarding the stability dissolve due to diffusion in *in vivo* conditions, where bodily fluidics are consistently present or in contact with implanted biomaterials.<sup>[24–26]</sup> A stretchable and long-lasting anti-fouling surface for implantable medical devices and bioelectronics still needs to be developed. Moreover, superhydrophobic surfaces require complex fabrication processes to form nano-microstructures and silane-based functionalization.<sup>[27]</sup> Thus, there are still unmet challenges to implementing superhydrophobic surface modification in medical implants and bioelectronics.

To overcome the limitations of stability for superhydrophobic surface modification, a lubricant-infused surface was developed, inspired by the surface characteristics of the *Nepenthes* pitcher plant.<sup>[28,29]</sup> The slippery liquid lubricant fills the nano-microstructure, exhibiting extreme liquid-repellent characteristics with long-term stability under physiological conditions. This phenomenon could be attributed to chemical affinity and matching interfacial energy between the lubricant and the low-surface energy of the silanized surface. However, the silanized surface is vulnerable to mechanical stresses, especially stretching motions, as the distances between each silane monomer increase.<sup>[30]</sup> Recently, the fabrication of a liquid-infused surface was reported, which utilized a lubricant swellable perfluoropolymer layer.<sup>[31]</sup> However, it was observed to crack under stretching conditions. These cause local instability in interfacial energy, leading to the degradation of liquid-repellent properties. Therefore, the implementation of lubricant-infused surfaces in soft bioelectronics has been challenging due to the loss of coating characteristics under flexible and stretching conditions.

In this study, we introduce a lubricant-infused (poly(1,3,5,7-tetramethyl-1,3,5,7-tetravinyl cyclotetrasiloxane) (V4D4)) interface with a perfluoropolymer (L-VIP) that exhibits stable anti-fouling properties under stretching. The coating was developed by utilizing a UV-curable and stretchable adhesive-perfluoropolymer bilayer consisting of a stretchable adhesive polymer V4D4 and a perfluoropolymer (1H,1H,2H,2H-perfluoroctyl methacrylate (FOMA)). The stretchable bilayer exhibits a strong affinity for perfluoropolyether-based lubricants, resulting in exceptional anti-fouling and slippery properties. Perfluoropolyether-based lubricants offer numerous advantages, including biocompatibility and anti-fouling capabilities. The L-VIP coating can be applied to various materials, including paper tissue, fabric, steel, polymer-based plastics, and even hydrogels, due to its shorter coating process. The coating also maintains its anti-fouling properties after repeated stretching cycles (>2000 cycles at 150% strain), and exposure to various stressors such as mechanical, aqueous, temperature, and pressure. Furthermore, the L-VIP coating demonstrates its ability to effectively coat materials with high roughness or irregularity, such as paper tissue. Additionally, we evaluated the stability of the L-VIP coating *in vivo* by implanting L-VIP-coated PVA hydrogel into the subcutaneous skin of mice for a duration of 1 week.

Anti-fouling performance was verified against bacteria (*Staphylococcus aureus*, *Escherichia coli*), FBR-related cells, and proteins (fibroblast, albumin, fibrin). Finally, we assessed the biocompatibility of the L-VIP coated polyvinyl alcohol (PVA) hydrogel by implanting it into the subcutaneous skin of mice's back and hindlimb, which experience the most deformation in implanted materials. Histological results, including inflammatory response, macrophage density, and collagen wrapping, indicated a low FBR in L-VIP coated PVA hydrogel after one and four weeks of implantation.

## 2. Results

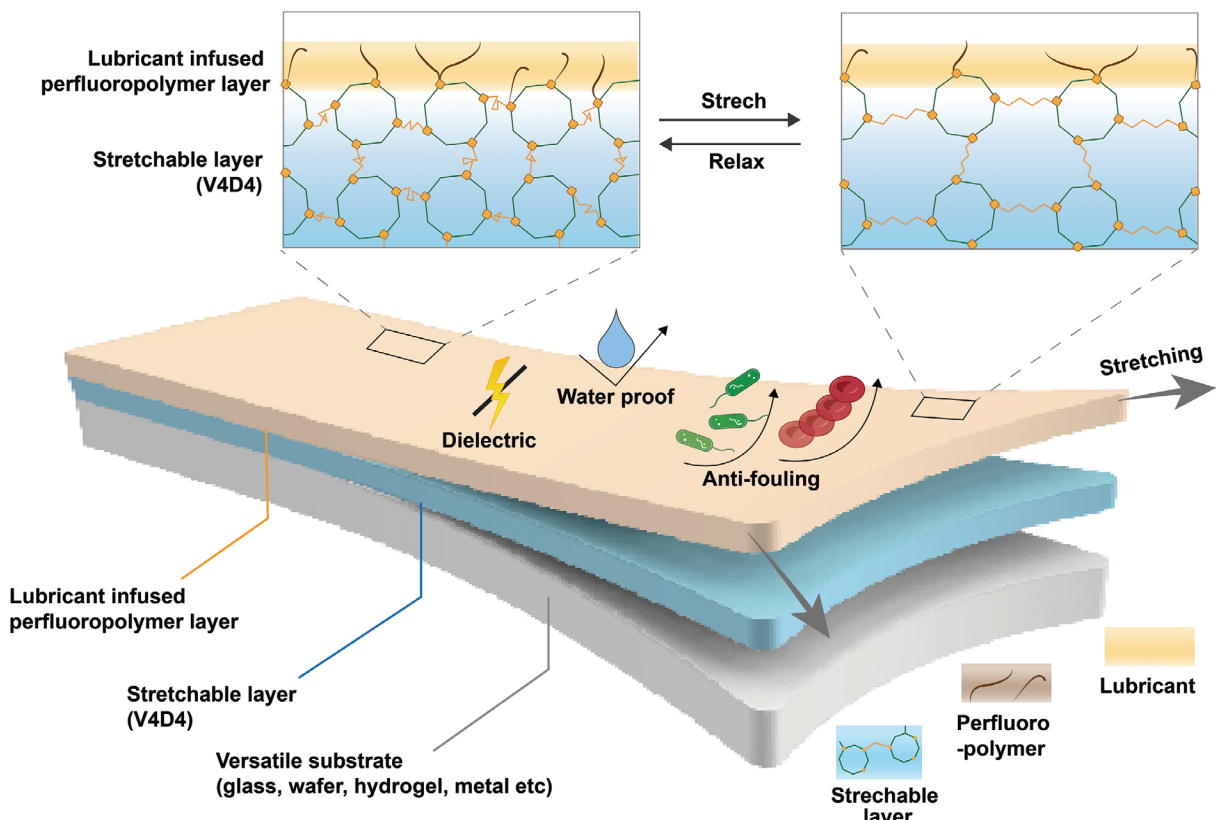
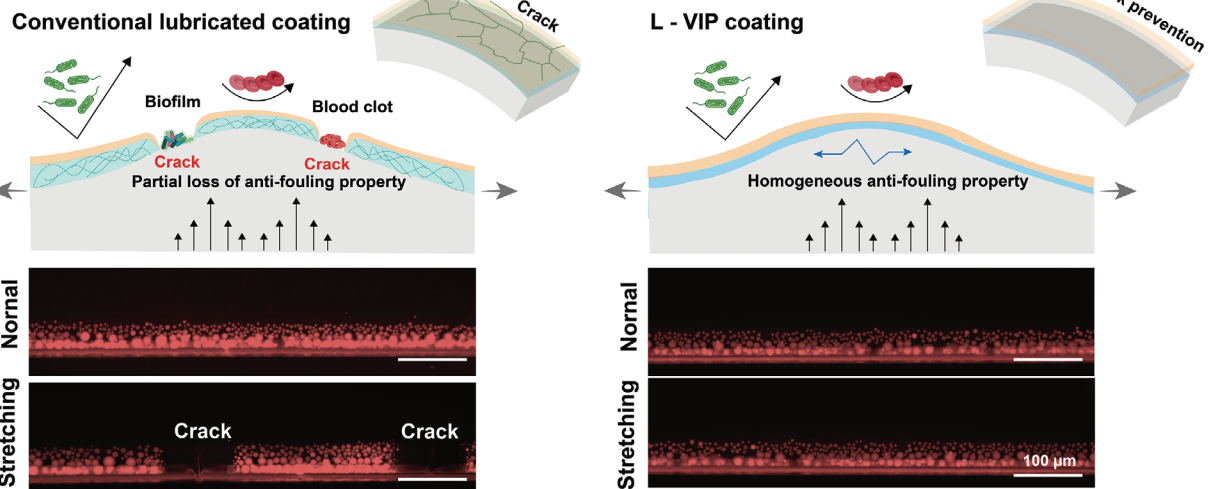
### 2.1. Development of Stretchable Anti-Fouling Coating

Figure 1a shows a schematic of the L-VIP coating, which exhibits fouling resistance, dielectric, waterproof, and stretchable properties, along with mechanical robustness, enabling it to withstand dynamic *in vivo* environments for extended periods. The L-VIP coating consists of three distinct layers: an adhesive and stretchable V4D4 layer, a perfluoropolymer (FOMA) thin film, and a perfluoropolyether-based lubricant layer. The V4D4 layer is an organosilicon-based stretchable adhesion layer with four vinyl functional groups (-CH = CH<sub>2</sub>) in each monomer. The abundant vinyl groups enable adherence to various materials and propagate themselves through radical photopolymerization using the photoinitiator 2,2-dimethoxy-2-phenylacetophenone (DMPA). The polymerization by reacting with the unsaturated bonds of the V4D4 monomers renders stretchability due to its omnidirectional covalent bond. The design of cross-linked V4D4 polymer aims to create an elastomeric material capable of undergoing substantial deformation under mechanical stress while exhibiting shape recovery. The elastomeric nature of the cross-linked V4D4 polymer demonstrates inherent molecular flexibility within its polymer chains, facilitating conformational changes and molecular rearrangements.<sup>[32–34]</sup> These characteristics contribute to the material's stretchability and ability to deform under applied stress. Additionally, the FOMA polymer, terminated with methacrylate groups (-CH<sub>2</sub>-CHCOO-), covalently binds to the vinyl groups of V4D4 by directly attaching to the carbonyl carbon atom of methacrylate groups of FOMA (Figure S1, Supporting Information).<sup>[35,36]</sup> The FOMA thin film possesses a strong chemical affinity to a perfluoropolyether-based lubricant due to similar chemical structures, thus having matching surface energy.<sup>[37]</sup> These allow lubricant infusion into the FOMA layer providing frictionless, waterproof, and fouling resistance properties. By combining the three layers, L-VIP demonstrates stretchability, fouling resistance, and dielectric properties with its slippery and frictionless surface. Figure 1b shows the conventional silanized lubricant-infused surface and L-VIP coatings under uniaxial strain conditions. Due to its excellent stretchability, L-VIP can exhibit fouling resistance properties on flexible and stretchable materials, making it suitable for soft bioelectronic applications. The coatings' ability to retain the lubricant was tested under normal and 150% strain conditions using confocal microscopy. The colorized perfluoropolyether-based lubricant with rhodamine B was infused into the stretchable adhesive-FOMA bilayer on the polydimethylsiloxane (PDMS) substrate.<sup>[38]</sup> The confocal microscopy images in normal conditions demonstrated ex-

cellent stability for both coatings. However, under stretching conditions, the conventional non-stretchable lubricant-infused surface coating exhibited crack formation, whereas the L-VIP coating maintained stable coating sustainability without any crack formation. Generally, partial damage and cracking of the anti-fouling coating can lead to local adhesion of bio substances, resulting in bacterial infection, FBR, and the loss of insulating properties in soft electronics. As lubricant-based coatings also function as insulators, crack formation in the coating disrupts airtight encapsulation, causing leakage current to the adjacent tissues. The results indicate that the stretchability of the L-VIP coating overcomes the limitations of conventional anti-fouling coatings with its exceptional robustness. This indicates that the L-VIP coating can be applied to implantable soft bioelectronics, offering stretchability and anti-fouling properties.

### 2.2. L-VIP Coating Characterization

Figure 2a shows the step-by-step fabrication process of the thin film of L-VIP coating via sequential photoinitiated. Changes in the chemical characteristics caused by surface functionalization were confirmed using X-ray photoelectron spectroscopy (XPS) (Figure S2, Supporting Information). The evaluation of the stretchable mechanism was conducted using Fourier Transform Infrared (FT-IR) spectroscopy measurements (Figure S3, Supporting Information). FT-IR spectroscopy assesses the interaction between infrared light and the sample materials, allowing for the evaluation of functional groups and their stretching or bending vibrations, potentially leading to changes in absorbance.<sup>[39]</sup> When the material undergoes stretching or bending vibrations, it induces alterations in the energy levels of the involved molecular bonds, subsequently influencing the material's absorption properties. Consequently, the absorbance of V4D4 at specific frequencies undergoes changes, indicating the presence of energy modification induced by stretching. Various kinds of organosilicone-perfluoropolymers bilayer coatings have been developed over the past decades.<sup>[32,40]</sup> The adhesive and stretchable organosilicone (e.g., V3D3 and V4D4) form highly cross-linked networks of themselves as well as methacrylate groups present in perfluoropolymers (e.g., PFOA and FOMA). The copolymerization of organosilicone-perfluoropolymers generates stretchable superhydrophobic polymer films due to their low surface energy. The copolymer films showed stretchability under a strain of 200% while maintaining the superhydrophobic properties. The fluorinated surface has chemical robustness, low adhesion, and fouling resistance against various materials with its lowering surface energy. However, organosilicone-perfluoropolymers bilayer coating has been reported as vulnerable to external mechanical damage and requires a long time for coating (more than an hour). To overcome these problems, we introduced ethanol and perfluoropolyether-based lubricant liquid. Ethanol serves as a solvent dissolving unwanted photoinitiator as well as medium that mixes V4D4 and FOMA homogeneously. The initial state of V4D4 and FOMA is a liquid phase. However, both chemicals do not mix and are separated due to their asymmetry in free energy, enthalpy, and entropy. By employing the ethanol, these two chemicals were homogeneously mixed which reduce the coating time dramatically to 10 min from hours.

**a****Lubricant - infused V4D4 Interface with Perfluoropolymer coating (L-VIP coating)****b**

**Figure 1.** Lubricated stretchable anti-fouling coating for versatile materials. a) Schematic of the lubricated V4D4 interfacial anti-fouling perfluoropolymer layer coating (L-VIP coating) composed of substrate, 1,3,5,7-tetravinyl-1,3,5,7-tetramethylcyclotetrasiloxane (V4D4), perfluoropolymer, and lubricant. b) Fluorescence microscopy images of conventional lubricated coating and lubricated VIP coated PDMS substrates substrate under 150% strain (scale bars, 100  $\mu$ m).

Perfluoropolyether-based lubricant liquid infusion to the bilayer renders the surface into a slippery and frictionless surface which protects it from external mechanical damage. To confirm the comprehensive applicability of the L-VIP coating, it was applied to various materials commonly used in biomedical fields, which

include polyvinyl alcohol (PVA) hydrogel, filter paper, wafer, PDMS, Ecoflex, polyvinyl chloride (PVC), polypropylene (PP), and aluminum alloy (AL5052). The L-VIP coated materials show similar static water contact angles (WCAs) regardless of their initial surface characteristics (Figure 2b). Next, we confirmed

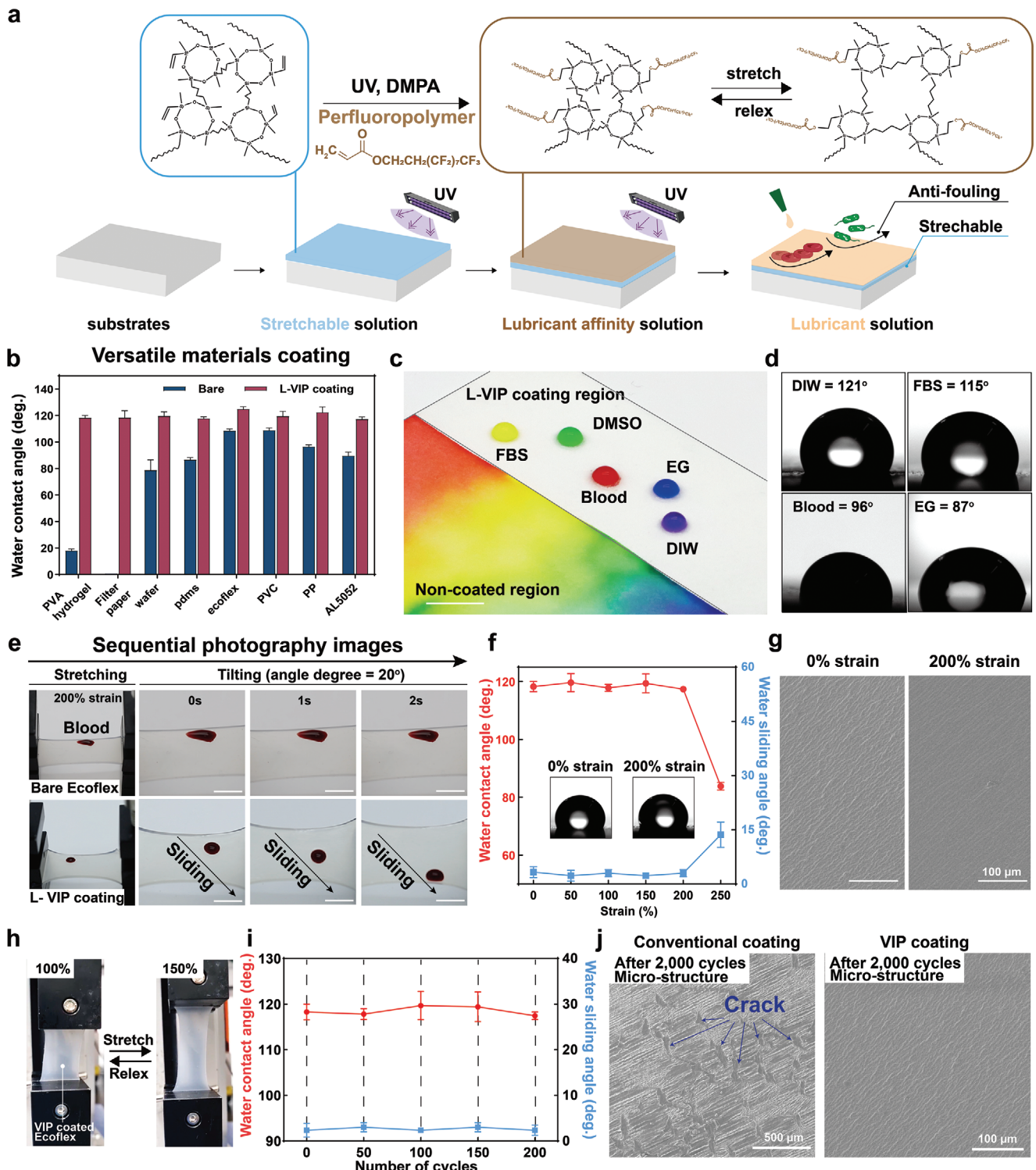


**Figure 2.** Fabrication process of L-VIP coating and its characterization. a) Schematic of the step-by-step fabrication process and square box demonstrate the principle of stretchability. b) Static water contact angle (WCAs) measurements of various material substrates on bare and L-VIP coated ( $n = 5$ ). c,d) Optical image and contact angles (CAs) measurement of various liquids on the bare and L-VIP coated filter paper (scale bars, 0.5 cm). e) Sequential photographs of blood droplets on bare, L-VIP coated Ecoflex substrate. Stretching up for 200% and tilted at 20° (scale bar: 2 mm). f, h,i) WCAs and water sliding angle (WSAs) on the L-VIP coated Ecoflex substrate under different uniaxial strains and the number of stretching cycles ( $n = 4$ ). g,j) SEM images of the VIP coated substrate under 200% strain and the number of stretching cycles (scale bar: 100  $\mu\text{m}$ ). (\* $P < 0.05$ , \*\* $P < 0.01$ , \*\*\* $P < 0.001$ , and \*\*\*\* $P < 0.0001$ ). ns, not significant.

fouling resistance performance with various liquids with different surface tension. The L-VIP coated filter paper exhibited extremely high liquid repellency for fetal bovine serum (FBS), dimethyl sulfoxide (DMSO), blood, ethylene glycol (EG), and deionized water (DIW). Conversely, the uncoated filter paper showed wettability against those liquids (Figure 2c). Additionally, we assessed the wetting behaviors of the L-VIP coated substrates by measuring the static contact angles (CAs) for different types of liquid droplets. The corresponding CAs are illustrated along with representative images (Figure 2d). The surface characterization result indicates that L-VIP applies to various materials used in biomedical applications and shows effective liquid-repellent properties against liquids with different surface tension. We conducted a comparative analysis between a previously reported biocompatible polyethylene glycol (PEG) based anti-fouling coating and L-VIP coating (Figure S4, Supporting Information). To assess their respective anti-fouling capabilities, L-VIP and PEG coated glass substrates were subjected to immersion in plasma proteins solution (albumin and fibrinogen). The PEG coating exhibited a relatively reduced protein adsorption compared to the bare glass substrate. Conversely, the L-VIP coated group displayed nearly complete anti-fouling capability, primarily attributed to its remarkably low surface tension. Additionally, a test involving the sliding of blood droplets along an inclined plane was performed. Only the L-VIP coated group demonstrated excellent repellency, leaving no residual traces of the blood droplets. The sequential images shown in Figure 2e demonstrate blood droplets on the slope while the bare and coated Ecoflex substrates are stretched to 200%. In the case of the bare Ecoflex substrate, the blood droplet was pinned onto the substrate and stretched along with Ecoflex. However, L-VIP coated Ecoflex was stretched without any defect formation, and liquid repellency against the blood droplets left no residues, even when stretched to 200% elongation. Figure 2f shows the surface characterization of static WCAs and water sliding angles (WSAs) for L-VIP coated Ecoflex under various strain conditions. The coating maintained WCAs  $\approx 120^\circ$  and WSAs less than  $8^\circ$  after the application of a uniaxial tensile strain, up to 200% strain. We noticed a decrease in WCAs and an increase in WSAs when the strain exceeded 200%, which was primarily attributed to the limited stretchability of the L-VIP coating. This phenomenon became evident when the strain surpassed the 200%, leading to partial defects, which, in turn, caused a reduction in WCAs and an increase in WSAs. It is noteworthy that these observations align with previous findings on similar stretchable coatings employing V4D4. The changes in surface morphology with the increasing tensile strain were observed using a scanning electron microscope (SEM) (Figure 2g). There were no significant differences in surface structure with or without tensile stress. Furthermore, the robustness of L-VIP coating against repeated stretching motions was tested. In these experiments, 150% uniaxial strain was applied and released in every cycle (Figure 2h). For quantitative analysis, WCAs and WSAs were measured after each repeated stretching of 1, 10, 100, 1000, and 2000 cycles (Figure 2i). The surface morphology of conventional lubricant-infused surface coating and L-VIP coating were demonstrated in the scanning electron microscopy (SEM) images. The SEM images showed no defect or crack formed on the L-VIP coating even after 2000 stretching cycles. Conversely, the conventional lubricant-infused surface coating exhibited various sizes of

cracks caused by uniaxial tensile strain (Figure 2j). The surface characterization of L-VIP coating indicates that the L-VIP coating applies to various materials showing liquid-repellency while withstanding strains.

### 2.3. Mechanical Robustness and Dielectric of the Coating

For practical applications, the mechanical robustness of the coating is crucial to bestow strong adherence to the target substrate. Usually, many kinds of developed anti-fouling coatings tend to fail in a moist environment and under extrinsic stresses.<sup>[41]</sup> To evaluate the mechanical performance, a standardized adhesion test was implemented using a crosscut test following ISO 2409 guidelines. VIP coated glass substrates were compared against a PEG-based anti-fouling coating as negative control and a poly-dopamine (PDA) coating as positive control. The red line indicate of the coatings (Figure S5, Supporting Information).<sup>[42]</sup> PDA is a well-known bioadhesive that demonstrates stable adhesion to various substrates without any delamination. Each test sample was cut using a cross cutter that has six cutting blades with 1 mm spacing to make a lattice of 25 small blocks of the coating which was indicated using red lines (Figure 3a). Then, the tape was attached and then peeled off horizontally to the surface. The optical images show the result of two different coatings: PEG-based coating and VIP coating. PEG-based coating maintained its structure soon after crosscut, but the coating started to peel off as the tape peeling was applied. However, VIP coating exhibits excellent adhesion where none of the blocks were detached. This is contributed to the strong C-C sigma bonding by photoinitiated crosslinking polymerization between V4D4 and FOMA layers, which significantly enhances the adhesion of the coatings. Figure 3b shows experiments to evaluate the mechanical durability of the coating under diverse aqueous external stresses. Subsequently, quantification analysis was performed to evaluate fouling resistance using a body fluidic molecule, humic acid, which is commonly found in the human body. The coated substrate was examined under various conditions. First, the L-VIP coated glass substrate was exposed for 1 day in a water ultrasonication bath (20 kHz) at room temperature. Second, L-VIP coated glass substrate was exposed to continuous perpendicular water flushing at a flow rate of  $5 \text{ mL s}^{-1}$  for seven days. Finally, L-VIP coated glass substrate was exposed to water shearing (1000 rpm) at room temperature for 30 days. Afterward, the substrates were incubated in a suspension of humic acid in PBS solution ( $5 \text{ mg mL}^{-1}$ ) for one day, followed by quantification analysis using UV-vis measurements at a range of 200 to 254 nm. Humic acid, a major component of the extracellular matrix (ECM), serves various functions in the human body, including its role in immune cell stimulation, molecule binding, facilitation of cell communication, and biofilm formation. Crucially, when compared performance of L-VIP coated glass to that of bare glass, our results revealed nearly identical fouling resistance both before and after exposure to three different conditions. These results affirm the stability of the L-VIP coating in the presence of various aqueous environments and physical stressors over an extended duration. Additionally, we conducted a chemical compatibility test using a PDMS-based microfluidic system (Figure S6, Supporting Information). PDMS is known to have poor chemical

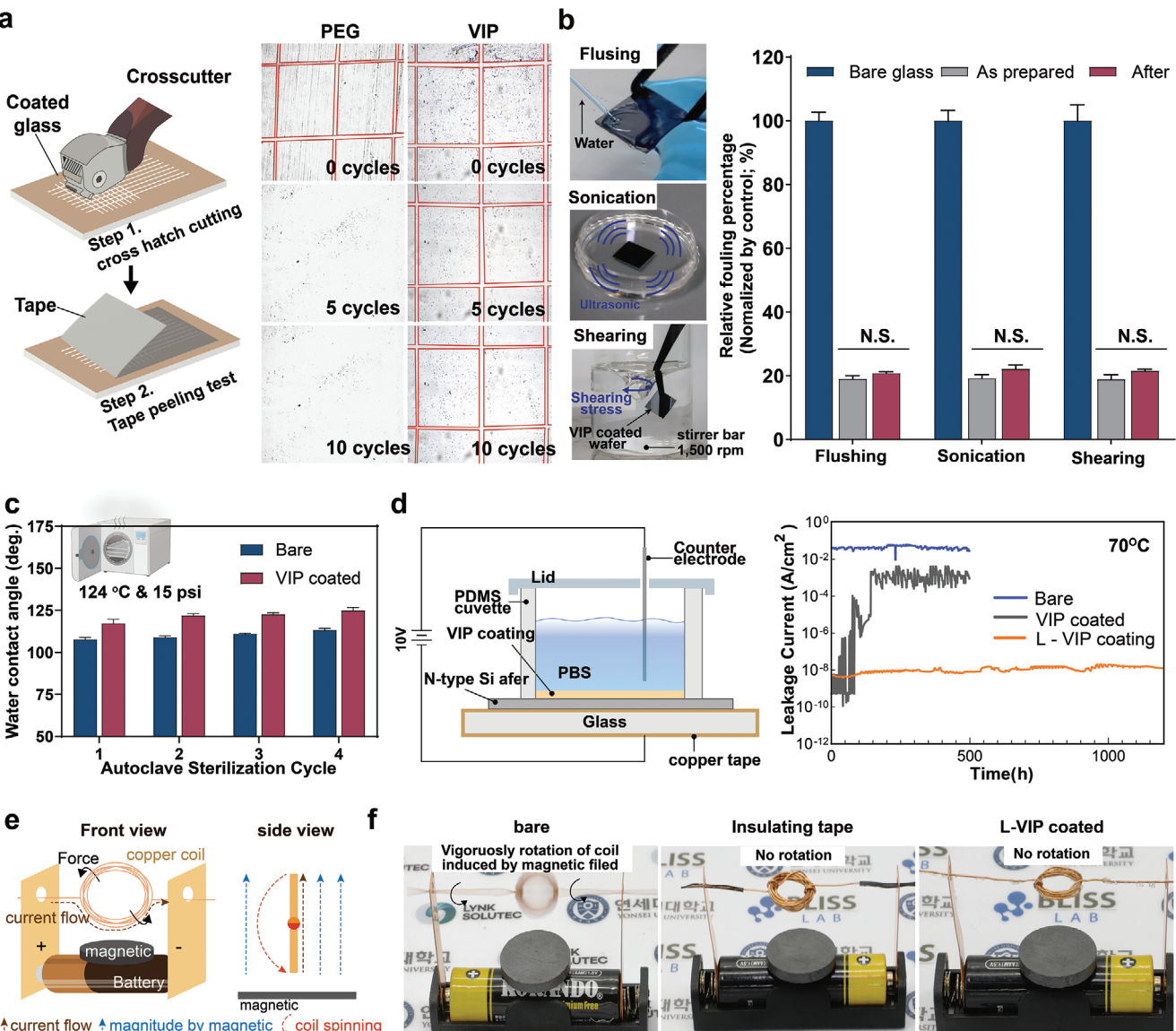


**Figure 3.** Mechanical robustness and effect of L-VIP coating on impedance. a) Schematics of cross-hatch cutting test (ISO 2409) and optical images of PEG and VIP coating after hatch cutting test. Red lines indicate the edge of the coatings ( $n = 3$ ). b) Anti-fouling properties of the L-VIP coating against body fluidic protein (humic acid) after various durability tests; 7 days exposure to perpendicular water flush, 1 day exposure to ultrasonication without temperature control, and 30 days exposure to water shearing ( $n = 4$ ). c) WCAs measurements of bare and L-VIP coated Ecoflex substrates after the number of autoclave sterilization cycles ( $n = 4$ ). d) Schematics of measurement of leakage current and leakage current of bare, VIP coating, and L-VIP coated Si wafer ( $n = 3$ ). e) Schematics of dielectric verification of L-VIP coated copper wire with simple rotation motor device. f) Dielectric performance of L-VIP coating compared with bare and insulating tape ( $n = 3$ ). (\* $P < 0.05$ , \*\* $P < 0.01$ , \*\*\* $P < 0.001$ , and \*\*\*\* $P < 0.0001$ ). ns, not significant.

stability, particularly with organic solvents like toluene. We flowed toluene through both the normal and L-VIP coated microfluidic channel walls to evaluate the chemical swelling behavior. The data obtained from this test demonstrate no chemical swelling of the L-VIP coated microfluidic system, indicating its stability and compatibility with the tested solvent. Autoclave sterilization, also known as steam sterilizer, is typically used for industrial or healthcare applications to clean harmful substances prior to clinical applications. The bare and L-VIP coated PDMS substrates were autoclaved nine times. Static WCAs were measured before and after the autoclave sterilizations to confirm the

degradation in its fouling resistance performance (Figure 3c). The WCAs measurements of both PDMS substrates were insignificant changes after the number of autoclaves. Dielectric performance in implantable bioelectronics is crucial because its leakage can cause unnecessary and intermittent tripping of implanted electrical devices and damage adjacent tissues.<sup>[43,44]</sup> The L-VIP coating act as an electrical passivation layer and prevent electrical current leakage into the interfacial biofluid. We monitored the electrical resistance of L-VIP coating, confirming leakage in the PBS solution. As shown in Figure 3d, we evaluated the dielectric performance of VIP coating with or without

perfluoropolyether-based lubricant infusion using leakage current measurement in accelerated aging conditions (at a temperature of 70° and constant voltage stress of 10 V s<sup>-1</sup>) with N-type Si wafer.<sup>[45,46]</sup> The VIP coated wafer without perfluoropolyether-based lubricant lost its dielectric performance after 36 h which was calculated to be 20 days at 37°C. In contrast, the L-VIP coating showed complete dielectric performance over 1200 h which was calculated to be almost two years in body-temperature conditions. Additionally, dielectric performance was examined using a simple rotation motor device which consists of copper wire, battery, and magnet (Figure 3e). When the current flowed, the bare copper coil vigorously rotated due to the one-direction force induced by the current following Fleming's rule. However, the L-VIP and insulating tape group showed no rotation due to its dielectric property (Figure 3f). The overall results suggest that the L-VIP coating is mechanically robust and that it is suitable for dynamic and moisture in vivo environments. Moreover, electrical characterization results suggest excellent dielectric performance as a coating layer for implantable bioelectronics. L-VIP coating could enable long-term implant bioelectronic application, thereby reducing the possibility of side-effect induced by the implants.

#### 2.4. Anti-Fouling Performance and Biological Effect

For the practical application of L-VIP coating in implantable soft bioelectronics, anti-bacterial infection, and FBR reduction are key factors to be assessed. The adhesion of biomolecules was compared to investigate the anti-biofouling properties. As shown in the fluorescence images in Figure 4a, the substrates were incubated in plasma proteins (albumin and fibrinogen) suspension and imaged. In the case of bare substrates, a relatively large number of proteins have adhered to their surface. However, the L-VIP coated substrate showed superior anti-fouling performance against plasma protein. Figure 4b shows the statistical analysis, which is calculated by fluorescence images using ImageJ/FIJI software program. L-VIP coated glass substrates also show excellent fouling resistance against the ECM components of biomolecules (Figure 4c). Each substrate was incubated in a suspension of several biomolecules (alginic acid, glucose, cholesterol, and humic acid). Among various ECM components, humic acid has been reported to stimulate biofilm formation due to its readily metabolized microbiota.<sup>[47]</sup> Biofilm is a 3D matrix consisting of complex communities of bacteria and their extracellular polysaccharides to form a tight network of microorganisms. Therefore, the result suggests that the L-VIP could be an effective measure to prevent bacterial biofilm formation on the implanted substrates. Then, we further investigated the anti-biofouling properties with the representative infectious pathogenic bacteria of gram-negative *Escherichia coli* (*E. coli*) and gram-positive *Staphylococcus aureus* (*S. aureus*). Both bacteria are recognized as the most common causes of biofilm formation and eventually result in surgical site infection.<sup>[48]</sup> Figure 4e,f shows the representative optical microscope images of colonies and colony-forming unit (CFU) measurements of each surface. The L-VIP coating exhibited virtually no bacteria adherence after 24 h of incubation because of its superior anti-fouling performance (Figure S7, Supporting Information). Many kinds of conventional hydrophilic polymer-based and perfluoropolymer-

based anti-bacterial coatings have been reported. However, hydration layers formed by hydrophilic polymers are often brittle and soluble in bacterial suspension due to their weak binding with water molecules.<sup>[49]</sup> In addition, the perfluoropolymer anti-bacterial coating is weak to external damage and a moisture environment. These limitations would result in bacterial adhesion and proliferation by coating layer depletion over long-term incubation. Conversely, the L-VIP coating can strongly bind with fluorinated lubricant to form a stable anti-fouling layer; therefore, effectively suppressing the bacteria adhesion. The result related to anti-biofouling properties suggests L-VIP's effective prevention of bacterial film formation. Moreover, the in vitro biocompatibility experiments of the coating were conducted to evaluate its nontoxicity for medical device applications. The L-VIP coated polyvinyl alcohol (PVA) hydrogel was incubated with NIH 3T3 fibroblasts using two distinct methods: indirect (transwell) and direct (submerge) approaches in cell culture media over a three-day period. The indirect cell biocompatibility test mimics a more physiological environment by enabling the separation of cells from direct contact with the tested material, thus simulating a realistic in vivo condition. However, this separation limits the assessment of direct cell-material interactions, which may be critical in certain applications. To address this limitation, we also conducted a direct cell biocompatibility test. Subsequently, a live/dead assay and cell counting kit-8 (CCK-8) assay were conducted to evaluate cell viability and proliferation (Figure 4h; Figure S8a-d, Supporting Information).<sup>[50]</sup> The result showed no effect on cell viability for L-VIP coated PVA hydrogel group. Additionally, cell morphological changes analyzed as cell morphology could be another biomarker to assess the biocompatibility of the materials.<sup>[51]</sup> When foreign material is implanted, activated inflammation causes fibroblasts to experience a morphological change from a healthy spindle shape to a pathological circular shape by remodeling the cytoskeleton.<sup>[52]</sup> We stained with TRITC phalloidin for actin filaments of NIH 3T3 fibroblasts. The aspect ratio ( $L_{\text{long}}/L_{\text{short}}$ ) was calculated using ImageJ/FIJI software program with a fluorescence image of fibroblasts with or without the L-VIP coated PVA hydrogel for five days (Figure 4i; Figure S8e, Supporting Information). The results demonstrated that L-VIP coating has no significant difference in cellular morphology change compared with the uncoated PVA hydrogel group.

#### 2.5. In Vivo Biocompatibility and Durability of the Coating

Before clinical application, the evaluation of in vivo biocompatibility is mandatory for applications in implantable materials. Given that L-VIP coating showed biocompatibility in vitro cell viability and morphological change analysis, in vivo subcutaneous implantation was conducted using female ICR mice, and its biocompatibility was investigated for up to four weeks. The bare and L-VIP coated PVA hydrogel were implanted into the subcutaneous dorsal and hindlimb skin of the mice. Both regions are the most physical deformation of implanted materials following animal daily movement (Figure 5a).<sup>[53,54]</sup> To evaluate the extent of a local acute inflammatory response, we examined the presence of cutaneous skin change in implanted sites. In bare and L-VIP coated PVA hydrogel of implanted sites, no abnormal cutaneous skin reactions, including swelling, erythema,

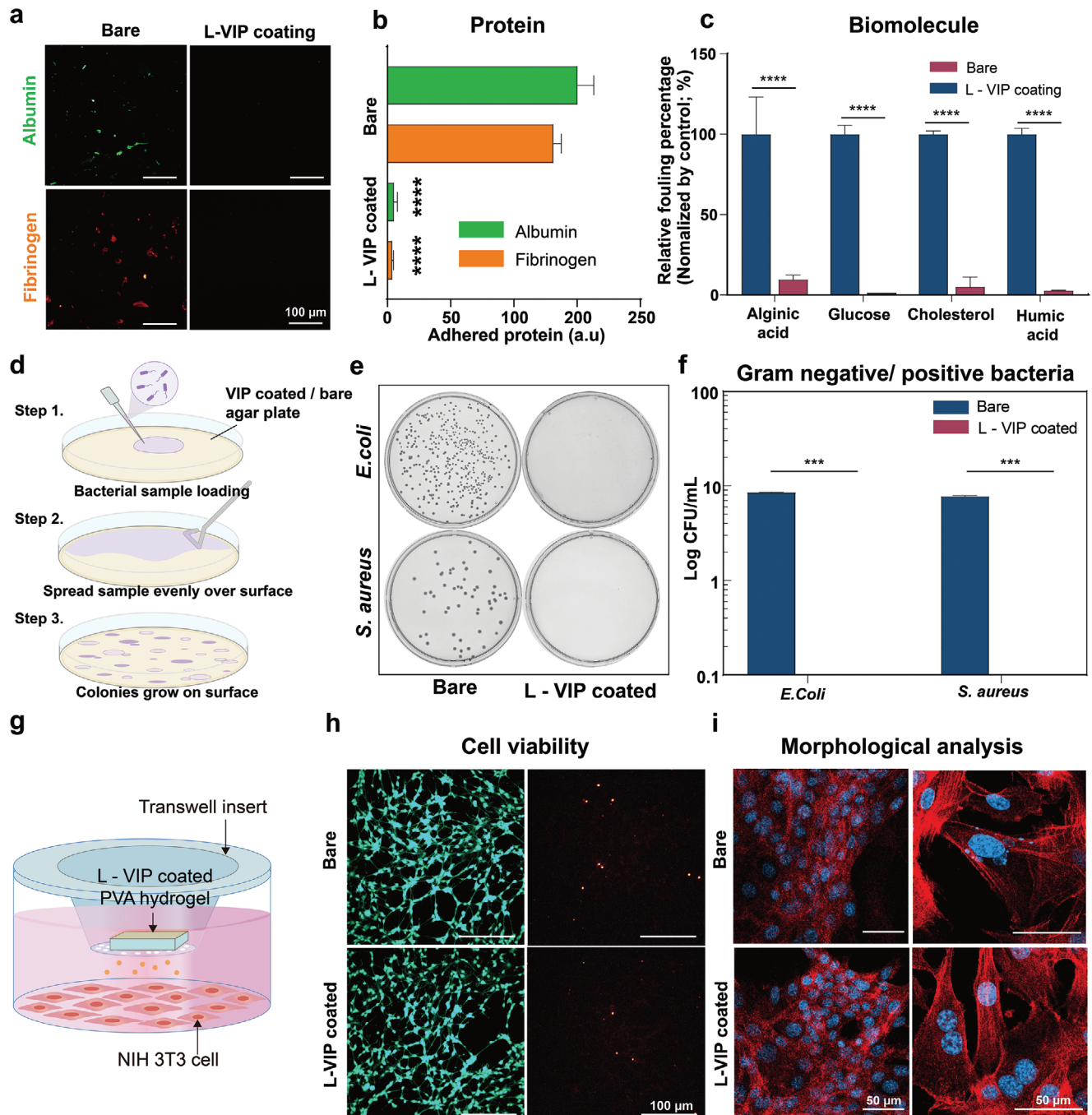


**Figure 4.** Anti-fouling performance of L-VIP coating and biological effects. **a,b)** Fluorescence microscopy images of plasma proteins (albumin and fibrinogen) adhered on bared and L-VIP coated substrates and statistical analysis of the protein coverage (scale bars, 100  $\mu$ m) ( $n = 4$ ). **c)** Relative fouling percentage of biomolecules ( $n = 5$ ). **d)** Schematics of bacterial test of bare and L-VIP coating. **e,f)** Optical images and the number of adhered CFUs of bare and L-VIP coating incubated in *E. coli* and *S. aureus* suspension for 24 h ( $n = 4$ ). **g)** Schematics of cell viability and morphological analysis test. **h,i)** Fluorescence microscopic images of NIH 3T3 cells of bare PVA hydrogels and L-VIP coated PVA hydrogel ( $n = 3$ ) (scale bars, 100 and 50  $\mu$ m). (\* $P < 0.05$ , \*\* $P < 0.01$ , \*\*\* $P < 0.001$ , and \*\*\*\* $P < 0.0001$ ). ns, not significant.

infiltration, blister, and ulcer, were observed (Figure S9, Supporting Information). This optical image demonstrated that both implants inflict no severe inflammation response to the implanted sites. To confirm the overall reaction ranging from FBR to fibrotic encapsulation of the implant, the adjacent skin surround-

ing the hydrogel was explanted one week after implantation, and subsequent histological and immunohistochemical analyses were conducted, including hematoxylin and eosin (H&E), Masson's trichrome (MT), and anti-F4/80 staining. We analyzed the explanted tissues through inflammatory response, macrophage

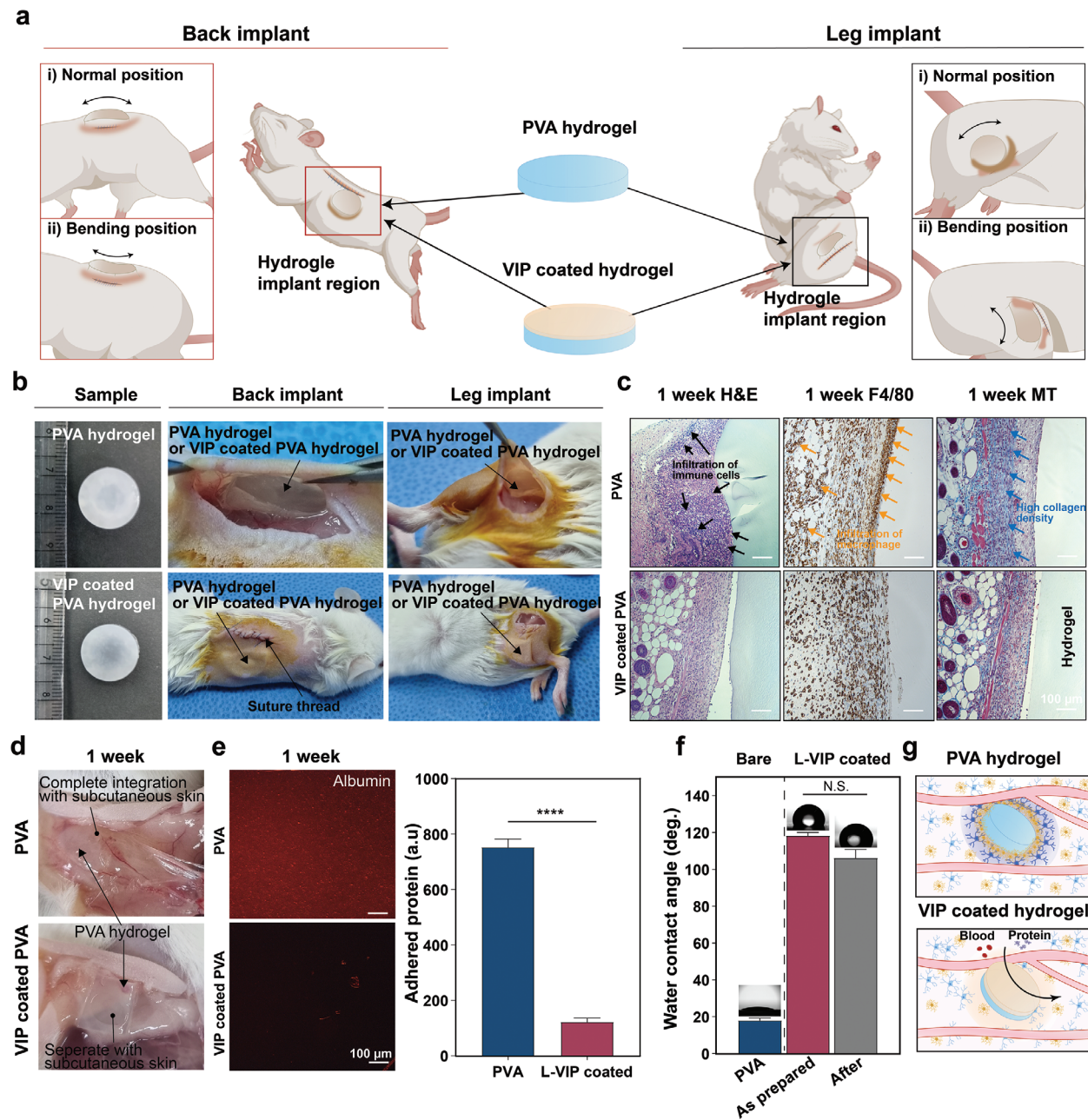


**Figure 5.** Evaluation of the in vivo biocompatibility and durability. a) Schematics of subcutaneous implantation of bare and L-VIP coated PVA hydrogels into the backs and hind legs of ICR mice. b) Optical image of hydrogels implantation. c) Histological analysis after one week of implantation: H&E (hematoxylin & eosin), nuclei were stained blue, and the cell cytoplasm were stained pink; F4/80, macrophage marker stained in brown; MT (masson's trichrome), collagen was stained in blue, nuclei were stained in black, and the cytoplasm was stained in red. The black arrows indicating: infiltration of immune cells, yellow arrows indicating: infiltration of macrophages, and blue arrows indicating: collagen densities ( $n = 3$ ) (scale bars, 100  $\mu$ m). d) Optical image of bare and L-VIP coated PVA hydrogels implantation after one week ( $n = 3$ ). e) Fluorescence microscopy images of plasma protein (albumin) adhered on bared and L-VIP coated substrates and statistical analysis of the protein coverage (scale bars, 100  $\mu$ m) ( $n = 3$ ). f) Optical image and WCAs measurements on the bare, L-VIP coated PVA hydrogel, and L-VIP coated PVA hydrogel after 1week implantation ( $n = 3$ ). g) Schematic of fibrotic encapsulation of bare and L-VIP coated PVA hydrogels. (\* $P < 0.05$ , \*\* $P < 0.01$ , \*\*\* $P < 0.001$ , and \*\*\*\* $P < 0.0001$ ). ns, not significant.

density, and collagen density at one and four weeks after implantation (Figure 5c; Figures S10 and S11, Supporting Information). The H&E staining exhibited inflammation around the bare PVA hydrogel, consistent with previous reports, and showed a low inflammatory response around the L-VIP coated PVA hydro-

gel. The F4/80 staining revealed a mass of murine macrophage cells (brown) in tissues around the bare PVA hydrogels. When FBR begins, the various types of macrophages are driven toward the implant. Subsequently, they become immobilized on the tissue/hydrogel interface. Therefore, the initial stage of FBR

gathers macrophages, which are the clear driving force of the final stage of FBR. The PVA hydrogel group generated thicker and high-density of macrophages in the tissue/hydrogel interfacial region, whereas a significantly lower density of macrophage cells was confirmed in explanted tissues surrounding the L-VIP coated PVA hydrogel (Figure S10a–c, Supporting Information). The final stage of FBR is fibrotic encapsulation of surrounding implants. Fibrotic encapsulation was generated by the recruitment of additional macrophages and fibroblasts, which promote the formation and deposition of collagen fibers. The MT staining demonstrated a relatively organized thick collagen (blue) layer surrounding the bare PVA hydrogel. In contrast, thin and inorganized low-density collagen was observed in the L-VIP coated hydrogel. L-VIP coating prevents the implant from FBR and fibrotic encapsulation with its superior anti-fouling properties and stability in dynamic in vivo conditions. The long-term coating sustainability was evaluated after implantation at four weeks. The bare PVA hydrogel was observed surrounded by numerous nuclei (dark brown) caused by FBR-related cells and encapsulated by a thick and highly dense layer of collagen (blue), whereas the L-VIP coated PVA hydrogel showed very low nuclei and density of collagen in the tissue surrounding the hydrogel (Figure S11, Supporting Information). The result demonstrates that the coating stably persists in dynamic in vivo conditions for the long term. Throughout the duration of implantation of foreign materials, various tissues are impacted, resulting in alterations in the weight and length of the spleen. The spleen, as a specialized immune organ, plays a significant role in innate and adaptive immunity. The spleen contains lymphoid tissue aggregates, which are closely associated with immune responses. Conditions such as infectious diseases can cause splenomegaly, characterized by an inflammatory response. Therefore, we monitored changes in spleen weight and length one and four weeks post-implantation. The optical image revealed no significant weight and length change in each experiment group, including sham and PVA hydrogel with or without L-VIP coating (Figures S10d–f and S12, Supporting Information). In addition, the H&E and F4/80 staining exhibited no difference between PVA hydrogel and L-VIP coated PVA hydrogel groups (Figure S10g,h, Supporting Information). The results demonstrate that overall immunity has no adverse effects by increasing the immune system. While some reports have raised concerns about the bioaccumulation and environmental persistence of perfluoropolymers, such as PFOA and PFOS, it is essential to note that these substances are commonly employed in significant quantities in various applications, including paints, photographic film additives, and textile finishing industry. In our study, we are working with a relatively small amount of perfluoropolymer, as evident from the presented data, which corresponds to  $\approx 100$  nm thin film (Figure S2c, Supporting Information). Therefore, we anticipate minimal environmental impact. Additionally, to assess the bioaccumulation of the coating in the liver, we conducted aminotransferase (ALT) and aspartate aminotransferase (AST) measurements after one week of implantation of L-VIP coated PVA hydrogels. The in vivo bioaccumulation of perfluoropolymers which occurs in the liver can lead to adverse effects, including elevated serum AST in relation to serum ALT. Our findings, which indicate similar ALT and AST levels after one week of implantation of PVA hydrogels with or without L-VIP coating suggest no significant

bioaccumulation in the liver (Figure S13, Supporting Information). Finally, we conducted a comprehensive evaluation of the in vivo stability of the L-VIP coating. After one week of implantation, the samples were carefully retrieved, and the L-VIP coated PVA hydrogels that were immersed in PFPE liquid to establish a lubricant-infused layer. Subsequently, an anti-fouling test using fluorescence-labeled albumin, along with static WCAs measurements, was performed. The representative optical image clearly illustrates the difference between the bare PVA hydrogel and the L-VIP-coated counterpart. The PVA hydrogel integrates completely with the subcutaneous skin tissue, while the L-VIP-coated group shows separation from the subcutaneous skin due to its inherent anti-fouling properties (Figure 5d). The L-VIP-coated PVA hydrogel exhibits exceptional anti-fouling capability against the plasma protein (albumin) in an adhesion test, as demonstrated by fluorescence labeling (Figure 5e). Furthermore, no significant differences were observed in the static WCAs before and after subcutaneous skin implantation, indicating the stability of the coating in in vivo condition (Figure 5f). As shown in Figure 5g, schematics depict the outcomes concerning the extent of FBR on PVA hydrogels, with and without L-VIP coating, following implantation. The hydrogel coated with L-VIP is expected to exhibit outstanding anti-fouling properties against bodily molecules, including blood components, FBR-associated proteins, and cells such as macrophages and fibroblasts. In contrast, the uncoated PVA hydrogel is likely to experience an initial deposition of bodily molecules and subsequently develop fibrotic encapsulation. The evaluation of in vivo biocompatibility, coating sustainability, and absence of adverse responses upon contact with tissue unequivocally support the potential of the L-VIP coating for soft bioelectronic applications.

### 3. Conclusion

This study developed a multifunctional highly stretchable anti-fouling coating possessing a slippery surface for the application of soft bioelectronics. Although there have been reported various anti-fouling coatings for bioelectronics, achieving multiple functionalities, including stretchability, robustness against external damage, high-water-content material coating, and dielectric, remained a challenge. Herein, we demonstrated a quick, simple yet effective coating strategy for soft materials, even hydrogel, which could bring a paradigm shift in soft bioelectronics applications. Furthermore, applications of L-VIP on all kinds of biomaterials used in biomedical devices were demonstrated. Such universal applications were possible by adhesive layer with terminated vinyl groups that firmly bonded with the FOMA of the methacrylate group. The similar surface energy makes strong affinity behavior between FOMA thin film and PFPE. The combination of three components allows it to possess an anti-fouling with a frictionless surface and contributes to the highly stretchable behavior of more than 200% elongation via the highly cross-link conjugated cycloorganosilicone structure of the V4D4 layer. Furthermore, high biocompatibility of in vitro and in vivo conditions and long-term sustainability without any effect on the adjacent tissue in dynamic in vivo conditions indicate the applicability of clinical application. Looking ahead, we are committed to exploring alternative liquids for large-scale applications to further minimize any potential environmental impact.

This encompasses addressing concerns related to persistence in soil, air, and water, as well as the potential for bioaccumulation. We envision that our L-VIP coating can be practically utilized in implantable soft bioelectronics owing to its possibility of application in almost all types of material coating, robust mechanical durability, high biocompatibility, and even dielectrics.

## 4. Experimental Section

**Synthesis of L-VIP Coating:** 1,3,5,7-tetravinyl-2,4,6,8-tetramethylcyclotetrasiloxane (V4D4) was purchased from Gelest. 1H,1H,2H,2H-perfluorooctyl methacrylate (PFOMA), 2,2-Dimethoxy-2-phenylacetophenone (DMPA), and acetone were purchased from Sigma-Aldrich. Perfluoropolyether (PFPE, Krytox GPL 101) was purchased from Chemours.

A stretchable and anti-fouling polymer of V4D4-FOMA (VIP) was synthesized via UV crosslinking polymerization in the form of a thin film on different substrate materials, including Eco-Flex, PDMS, glass, wafer, filter paper, and PVA hydrogel. First, the stretchable monomer solution was prepared by dissolving V4D4 (900  $\mu\text{L}$ ) and DMPA (10 mg) in acetone solution (100  $\mu\text{L}$ ). The substrates were immersed in the V4D4 solution, and then they were irradiated with UV light having wavelengths from 254 to 365 nm using a UV chamber (AhTech LTS, Korea) for 5 min. Second, the fluoropolymer, which has an affinity with fluorinated lubricant, was prepared by dissolving FOMA (900  $\mu\text{L}$ ) and DMPA (10 mg) in acetone solution (100  $\mu\text{L}$ ). V4D4 deposited substrates were immersed in the FOMA solution, and then they were irradiated with UV light having wavelengths from 254 to 365 nm for 5 min. The VIP-coated samples were immersed in the PFPE liquid to form a lubricant-infused layer. Excess liquid was removed by tilting at 30° for 10 min before using. Prior to usage, unwanted substances were eliminated from PFPE by passing it through a syringe filter with a pore size of 0.22  $\mu\text{m}$ .

### Crack Formation Test

For micro-scale PDMS membrane fabrication, the ratio between base polymer (Sylgard 184, Dow Corning) and curing agent of 10:1 (w/w) were mixed and degassed in a vacuum desiccator. Then 1 mL of its mixture is poured on a wafer with a diameter of 135 mm. The PDMS micro-scale thick membrane is made using a spin coater (ACE-200, DongAh Tech. Korea) at 1000 rpm for 15 s, followed by a heat curing temperature of 70°C for 2 h, and gently peeling off. The fabricated PDMS membrane was coated with non-stretchable PFP and stretchable VIP coating. Then, colorized PFPE with rhodamine B was infused with each group. Subsequently, the uniaxial tensile strain was applied under 150% strain.

### Blood Fouling Test under Stretchability Test

The blood fouling test was performed using defibrinated horse blood (Kisanbio, Korea) in bare and L-VIP coated Ecoflex substrate. 10  $\mu\text{L}$  droplets of the blood were dropped on each group, and the uniaxial tensile strain was applied under 200% strain. Then the blood-loaded Ecoflex was tilted at an angle of 20°.

**Characterization of L-VIP Coating:** The surface structure of the substrates in each condition was investigated using a field emission scanning electron microscope (FE-SEM, JEOL, JSMT-500HR). Contact angle (CA) and sliding angle (SA) in static conditions were measured on bare, and L-VIP coated PDMS substrates were measured using a CAs measurement system equipped with a dynamic image capture camera (SmartDrop standard plus, FEMTOBIOMED. Inc.). 10  $\mu\text{L}$  droplets of various liquids (DI water, defibrinated horse blood (Kisan Bio), DMSO, acetone, ethylene glycol, and ethanol (Sigma-Aldrich) was loaded on the substrate to measure CAs. SAs of various liquid droplets were measured when the droplets start to roll with the substrate tilted for one degree per second. Similarly, CAs and SAs were measured on bare, and L-VIP coated versatile materials such as PVA hydrogel, glass, wafer, PDMS, Ecoflex, polyvinyl chloride (PVC), polypropylene (PP), and aluminum (AL5052). X-ray photoelectron spectroscopy (XPS, PHI 5000 VersaProbe, ULVAC PHI) was used to analyze surface chemical composition. The XPS was equipped with an Al K-alpha X-ray source possessing a spot size of 100  $\mu\text{m}^2$ .

**Mechanical Durability:** The mechanical flexibility was evaluated with VIP coated Ecoflex using repeated cyclic stretching at 150% strain for up to 2000 cycles. The mechanical durability of L-VIP was tested according to the cross-cut adhesion test (ISO 2409). The mechanical durability evaluation was tested using the cross-cut test. Two sets of six cuts with a spacing of gap between 1 mm were made perpendicular to each other to create a grid of 25 small blocks on the samples, including PEG-based anti-fouling coating as a negative control, PDA as a positive control, and VIP coated glass substrates. Afterwards, the adhesive tape was affixed to the surface and subsequently removed by peeling it at a 90° angle. The tape-peeling was repeated ten times. For durability evaluation of the aqueous environment, the VIP coating fouling resistance was measured before and after exposing it to ultrasonication, water-flushing, and water-shearing treatment. In the ultrasonication experiment, the L-VIP coated glass substrate was placed on a petri-dish and immersed in PBS. Then, the petri-dish with the PBS-immersed samples was placed in an ultrasonication bath and conducted with a frequency of 20 kHz without temperature control. In the water-flush experiment, A peristaltic pump was utilized to cycle DIW perpendicularly over the L-VIP coated glass substrate, with a flow rate of 5  $\text{mL s}^{-1}$ . In the water shearing test, the L-VIP coated glass substrate was placed on the inner center of the beaker and immersed in PBS before being subjected to shear rates (1000 rpm) induced by a magnetic stirring bar. Afterward, the substrates were incubated in a suspension of humic acid in PBS solution (5 mg  $\text{mL}^{-1}$ ) for one day, followed by quantification analysis using UV-vis measurements at a range of 200 to 254 nm.

**Sterilization Test:** Autoclave sterilization was performed to test the sterilization resistance of LVIP coating. Autoclave sterilization under the pressure of  $\approx$ 15 pounds and temperature of 121°C was conducted three, six, and nine times on each sample.

**Dielectric Test:** The leakage current measurement at an accelerated aging condition was confirmed using a probe station (MST 4000, MS Tech.) at 10 V. The VIP deposited an N-type Si wafer, and the PFPE was infused in the same way as described before. The glass substrate was covered with copper tape, and electroconductive silver paste (Elcoat P-100, Japan) was applied to the back side of the wafer. Then, adhere between copper tape covered glass and prepared wafers. Afterward, the prepared copper tape covered glass and the wafer complex adhered with hollow PDMS cuvette through the epoxy adhesive. Finally, PBS buffer was poured into the PDMS cuvette, and a piece of plastic lid sealed the top surface, preventing the evaporation of the PBS. Additionally, dielectric performance was measured using a simple rotation motor device which consists of copper wire, battery, and magnet. To prepare a bare enamel coil, an enamel wire is rolled into a cylindrical shape 10 times, leaving  $\approx$ 2 inches of straight wire on both side of the coil. The straight wire sections were then thoroughly sanded using sandpaper to remove the insulating layer of enamel from the coil. The enamel coil was prepared in three 3 variations: bare, insulated with tape, and coated with L-VIP. Subsequently, 2 copper plates were connected vertically to the positive and negative terminals of the battery. The prepared enamel coil was then inserted between these copper plates.

**Protein Adsorption Test:** Alexa Fluor 488 conjugated albumin from bovine serum (BSA; A13100, Invitrogen) and fibrinogen from human plasma (F13191, Invitrogen) were purchased from Invitrogen. The capacity of L-VIP coating to resist adhesion to plasma proteins was exhibited by immersing bare and L-VIP coated PDMS in 5 mL of aqueous protein solutions (1 mg  $\text{mL}^{-1}$ ) and then incubating them at 37 °C for 24 h. Following that, the specimens were rinsed with DI water and air-dried under ambient conditions. The protein adsorption on thePDMS was characterized using an inverted fluorescence microscope (IX81, Olympus, Japan) and quantified by the ImageJ/Fiji software program. A mixture of 10 g of PDMS and a base polymer to curing agent ratio of 10:1 (w/w) was degassed in a vacuum chamber and subsequently poured gently into a square polystyrene Petri dish (140 mm in diameter). The PDMS substrate was then cured in an oven at 70°C for a period of 2 h.

**Bacterial Preparation and Fouling Assay:** The anti-bacterial evaluation was performed with *E. coli* (ATCC 8739) as model gram-negative bacteria and *S. aureus* (ATCC 6538) as model grampositive bacteria donated by the Korean Agricultural Culture Collection (jeonbuk, Korea). The strain was cultured on a constant temperature shaker (37°C, 100 rpm)

for 12 h after dilution in sterilized Luria-Bertani (LB) broth. The original bacterial solution was diluted to a concentration of  $10^5$  cells  $\text{mL}^{-1}$  in the LB broth and subsequently dropped onto the surface of the agar plate. The sample was cultured at  $37^\circ\text{C}$  for 24 h, and the biofilm grew during the bacterial reproduction process. Afterward, the sample was slightly washed five times using PBS to remove the bacteria and plated for colony counting. The bacterial biofilm was fixed with methanol and stained with the Live and Dead staining kit for 15 min under dark conditions (LIVE/DEAD BacLight Bacterial Viability Kit, ThermoFisher, China). The kit is comprised of SYTO 9 (Merck) and propidium iodide (PI) to observe the biofilm on the substrate. Laser scanning confocal microscopy was employed to capture an image of the biofilm after it had been stained.

**In Vitro Biocompatibility Evaluation:** The PVA hydrogel (dissolved into DIW at a concentration of 8% (V/V)) was prepared through a repeated cyclic freeze-thaw (FT) process, according to a previous report. The PVA hydrogel was prepared with dimensions of  $15 \text{ mm} \times 15 \text{ mm} \times 0.5 \text{ mm}$  and coated with L-VIP. Afterward, a tow-chamber Transwell system ( $8 \mu\text{m}$  pore size; Corning) was used for cell viability and morphological change analysis. The prepared hydrogels were placed on the transwell insert. The NIH-3T3 fibroblast cells ( $0.5 \times 10^5$  cells  $\text{mL}^{-1}$ ) were cultured in 2 mL of DMEM supplemented with 10% bovine calf serum and 1% penicillin-streptomycin. Cell viability was evaluated using a Live/Dead kit (L3224, Invitrogen, USA) according to the manufacturer's instructions. Visualization of the cell viability was obtained using an inverted fluorescence microscope (IX81, Olympus, Japan) with a 10 $\times$  magnification. Similarly, morphological change was evaluated using aspect ratio calculation defined as the major cell axis divided by the minor one. For visualization, the actin cytoskeleton of fibroblast cells was stained using an Alexa 594-conjugated phalloidin (Thermo Scientific, Pittsburgh, PA, USA). The fibroblast morphology was observed using a confocal microscope (LSM 980, Carl Zeiss, Oberkochen, Germany) and calculated by the ImageJ/Fiji software program.

**Hydrogel Disk Implantation in Mice:** All animal experiments were conducted in accordance with the Guide for the Care and Use of Laboratory Animals and were approved by the Institutional Animal Care and Use Committee (IACUC) of Yonsei University (authorization number; IACUC-A-202210-1556-01 (mice)). Female ICR mice (7 weeks of age) were offered from Orient Bio Inc. (Gyeonggi-do, South Korea), and they were then quarantined under semispecific pathogen-free (semi-SPF) conditions with a 12 h light/dark cycle. The bare and L-VIP coated PVA hydrogels were prepared similarly as previously reported. Afterward, each sample was implanted into the left side of the mice's back and the right side of the mice's leg subcutaneous skin subcutaneously in ICR female mice, respectively. Briefly, mice were initially anesthetized by intramuscular injection of ketamine ( $100 \text{ mg kg}^{-1}$ ; Yuhan, Seoul, Korea) and xylazine ( $20 \text{ mg kg}^{-1}$ ; Bayer Korea, Ansan, Korea) and shaved. Then,  $\approx 15 \text{ mm}$  of longitudinal incision was made on the skin surface using surgical scissors to access the subcutaneous space where subcutaneous pockets were created on either side of the incision using blunt forceps to implant hydrogel disks. After implantation, the incisions were closed using a surgical suture thread. Mice were monitored and housed for one to four weeks.

**In Vivo Biocompatibility Evaluation:** After one week or four weeks, mice were sacrificed, and the surrounding tissue, along with the hydrogel samples, were extracted and gathered. The explanted samples were fixed in 4% paraformaldehyde (PFA) overnight at room temperature and embedded in paraffin wax. Sections of each sample at ( $3$  to  $5$ )  $\mu\text{m}$  thickness were cut and mounted onto slides for histological staining. The inflammatory response was examined by staining the tissue sections with hematoxylin and eosin (H&E), which stains nuclei in blue and cell cytoplasm in pink. Collagen formation and organization were stained using Masson's trichrome that stains collagen in blue, cytoplasm in red, nuclei in dark red or purple, and cytoplasm in red or pink. All images were scanned in a bright field inverted fluorescence microscope (IX81, Olympus, Japan). The collagen density is measured by the percentage of blue-pixel coverage in the Masson images within  $200 \mu\text{m}$  (at  $20\text{-}\mu\text{m}$  steps) of the hydrogel-tissue interface. Before immunoassay, antigen retrieval, endogenous peroxidase or fluorescence

cancellation, and serum blocking were performed. To stain macrophage after one and four weeks of implantation, F4/80 antibody from cell signaling (F4/80 D2S9R XP Rabbit mAb No. 70 076) was used overnight at  $4^\circ\text{C}$ . The sections were washed three times with PBS and incubated with HRP-labeled goat antirabbit antibody from Servicebio (1:200; catalog no. GB23303) at room temperature for 60 min in a dark room. Sections were washed three times, dried slightly, and then incubated with a freshly prepared diaminobenzidine (DAB) chromogenic reagent kit (Servicebio, catalog no. G1211). The sections were counterstained in the nucleus with hematoxylin staining solution (Servicebio, catalog no. G1004) for 3 min and washed with water. Macrophages stained by the DAB reagent have brown nuclei, whereas other nuclei stained with hematoxylin are blue.

**Statistical Analysis:** Graphpad Prism software (Graphpad Software Inc., USA) was used to carry out statistical analysis. The unpaired t-test, ordinary two-way ANOVA, and Tukey's multiple comparison test were utilized to evaluate variations between groups, with individual variances calculated for each comparison. The levels of statistical significance are represented in the Figures as follows: \* $p < 0.05$ ; \*\* $p < 0.01$ ; \*\*\* $p < 0.001$ ; \*\*\*\* $p < 0.0001$ ; ns: not significant.

## Supporting Information

Supporting Information is available from the Wiley Online Library or from the author.

## Acknowledgements

This work was supported by the National Research Foundation of Korea (NRF) grant funded by the Korea government (MSIT) (Project numbers: NRF-2021M3H4A1A04092883; NRF-2022R1A2C4001652). [Correction added on December 28, 2023, after first online publication: a grant number has been corrected in this version.]

## Conflict of Interest

The authors declare no conflict of interest.

## Author Contributions

T.Y.K. contributed to this work as the first author. J.S. is listed as the corresponding author, considering their significant contributions. J.S. designed and directed the entire study. T.Y.K. led the experiments, analyzed the data, and prepared the figures. S.K., J.L., K.P., J.P., and S.A.K. collaborated on the in vitro studies, and S.An., S.Y.H. assisted in the animal studies. Anti-bacterial experiments were conducted by Y.K. S.-W.C., and J.J.C. contributed to the experimental design. J.S. drafted the manuscript with assistance from T.Y.K.

## Data Availability Statement

Research data are not shared.

## Keywords

biocompatibility, lubricant-infused, prevention of FBR, soft electronics, stretchable anti-fouling coating

Received: October 16, 2023

Revised: December 5, 2023

Published online: December 26, 2023

- [1] Y. Li, N. Li, N. De Oliveira, S. Wang, *Matter* **2021**, *4*, 1125.
- [2] T. Wang, M. Wang, L. Yang, Z. Li, X. J. Loh, X. Chen, *Adv. Mater.* **2020**, *32*, 1905522.
- [3] J. Park, Y. Lee, T. Y. Kim, S. Hwang, J. Seo, *ACS Applied Electronic Materials* **2022**, *4*, 1449.
- [4] K. W. Cho, S.-H. Sunwoo, Y. J. Hong, J. H. Koo, J. H. Kim, S. Baik, T. Hyeon, D.-H. Kim, *Chem. Rev.* **2021**, *122*, 5068.
- [5] C. W. Zhang, X. P. Hao, Q. Zheng, Z. L. Wu, *Advanced Sensor Research* **2023**, *2*, 2200069.
- [6] X. Peng, W. Wang, W. Yang, J. Chen, Q. Peng, T. Wang, D. Yang, J. Wang, H. Zhang, H. Zeng, *J. Colloid Interface Sci.* **2022**, *618*, 111.
- [7] Z. Sheikh, P. Brooks, O. Barzilay, N. Fine, M. Glogauer, *Materials* **2015**, *8*, 5671.
- [8] J. S. Vanepps, J. G. Younger, *Shock* **2016**, *46*, 597.
- [9] P. S. Stewart, T. Bjarnsholt, *Clin. Microbiol. Infect.* **2020**, *26*, 1034.
- [10] D. M. Higgins, R. J. Basaraba, A. C. Hohnbaum, E. J. Lee, D. W. Grainger, M. Gonzalez-Juarrero, *Am. J. Pathol.* **2009**, *175*, 161.
- [11] J. M. Anderson, A. Rodriguez, D. T. Chang, *Semin. in Immunol.*, Elsevier, USA, **2008**, *20*, p. 86.
- [12] J. Kzhyshkowska, A. Gudima, V. Riabov, C. Dollinger, P. Lavalle, N. E. Vrana, *J. Leukocyte Biol.* **2015**, *98*, 953.
- [13] S. Lowe, N. M. O'brien-Simpson, L. A. Connal, *Polym. Chem.* **2015**, *6*, 198.
- [14] A. Camós Noguer, S. M. Olsen, S. Hvilsted, S. Kiil, *J. Coat. Technol. Res.* **2016**, *13*, 567.
- [15] M.-H. Zhao, X.-P. Chen, Q. Wang, *Sci. Rep.* **2014**, *4*, 5376.
- [16] Y. Fang, J. Xue, S. Gao, A. Lu, D. Yang, H. Jiang, Y. He, K. Shi, *Drug Delivery* **2017**, *24*, 22.
- [17] F. Kawai, *Biopolymers Online: Biology• Chemistry• Biotechnology• Applications* **2005**, *9*, 267.
- [18] W.-C. Lai, W.-B. Liu, *Polymer* **2003**, *44*, 8103.
- [19] B. Mizrahi, X. Khoo, H. H. Chiang, K. J. Sher, R. G. Feldman, J.-J. Lee, S. Irusta, D. S. Kohane, *Langmuir* **2013**, *29*, 10087.
- [20] Y. A. Mehanna, E. Sadler, R. L. Upton, A. G. Kempchinsky, Y. Lu, C. R. Crick, *Chem. Soc. Rev.* **2021**, *50*, 6569.
- [21] K. Chae, W. Y. Jang, K. Park, J. Lee, H. Kim, K. Lee, C. K. Lee, Y. Lee, S. H. Lee, J. Seo, *Sci. Adv.* **2020**, *6*, eabb0025.
- [22] X. Hu, C. Tang, Z. He, H. Shao, K. Xu, J. Mei, W.-M. Lau, *Small* **2017**, *13*, 1602353.
- [23] M. S. Oh, M. Jeon, K. Jeong, J. Ryu, S. G. Im, *Chem. Mater.* **2021**, *33*, 1314.
- [24] G. B. Hwang, K. Page, A. Patir, S. P. Nair, E. Allan, I. P. Parkin, *ACS Nano* **2018**, *12*, 6050.
- [25] M. A. Samaha, H. V. Tafreshi, M. Gad-El-Hak, *Langmuir* **2012**, *28*, 9759.
- [26] M. J. Hoque, S. Sett, X. Yan, D. Liu, K. F. Rabbi, H. Qiu, M. Qureshi, G. Barac, L. Bolton, N. Miljkovic, *ACS Appl. Mater. Interfaces* **2022**, *14*, 4598.
- [27] J. Li, E. Ueda, D. Paulssen, P. A. Levkin, *Adv. Funct. Mater.* **2019**, *29*, 1802317.
- [28] M. Tenjimbayashi, S. Nishioka, Y. Kobayashi, K. Kawase, J. Li, J. Abe, S. Shiratori, *Langmuir* **2018**, *34*, 1386.
- [29] D. Wang, Z. Guo, *New J. Chem.* **2020**, *44*, 4529.
- [30] Y. Yoo, J. B. You, W. Choi, S. G. Im, *Polym. Chem.* **2013**, *4*, 1664.
- [31] Y. Lee, H. Shin, D. Lee, S. Choi, I.-J. Cho, J. Seo, *Adv. Sci.* **2021**, *8*, 2100231.
- [32] M. S. Oh, J. Ryu, M. Jeon, I. Lee, B.-S. Bae, J. B. You, S. G. Im, *Adv. Mater. Interfaces* **2022**, *9*, 2201019.
- [33] S. Panyukov, *Polymers* **2020**, *12*, 767.
- [34] K. Mayumi, C. Liu, Y. Yasuda, K. Ito, *Gels* **2021**, *7*, 91.
- [35] H. S. Lee, H. Kim, J. H. Lee, J. B. Kwak, *Coatings* **2019**, *9*, 430.
- [36] G. Cihanoglu, Ö. Ebil, *J. Mater. Sci.* **2021**, *56*, 11970.
- [37] K. Park, S. Kim, Y. Jo, J. Park, I. Kim, S. Hwang, Y. Lee, S. Y. Kim, J. Seo, *Bioactive Materials* **2023**, *25*, 555.
- [38] M. Villegas, Y. Zhang, N. Abu Jarad, L. Soleymani, T. F. Didar, *ACS Nano* **2019**, *13*, 8517.
- [39] H. T. Ahmed, O. G. Abdullah, *Results in Physics* **2020**, *16*, 102861.
- [40] J.-H. Kim, S. K. Park, J.-W. Lee, B. Yoo, J.-K. Lee, Y.-H. Kim, *Journal of the Korean Physical Society* **2014**, *65*, 1448.
- [41] H. Kim, Y. Song, S. Park, Y. Kim, H. Mun, J. Kim, S. Kim, K. G. Lee, S. G. Im, *Adv. Funct. Mater.* **2022**, *32*, 2113253.
- [42] R. Arrabal, J. M. Mota, A. Criado, A. Pardo, M. Mohedano, E. Matykina, *Surf. Coat. Technol.* **2012**, *26*, 4692.
- [43] W. Wu, X. Liu, Z. Qiang, J. Yang, Y. Liu, K. Huai, B. Zhang, S. Jin, Y. Xia, K. K. Fu, J. Zhang, Y. Chen, *Compos. Sci. Technol.* **2021**, *216*, 109070.
- [44] G. Balakrishnan, J. Song, C. Mou, C. J. Bettinger, *Adv. Mater.* **2022**, *34*, 2106787.
- [45] K. Kim, M. Van Gompel, K. Wu, G. Schiavone, J. Carron, F. Bourgeois, S. P. Lacour, Y. Leterrier, *Small* **2021**, *17*, 2103039.
- [46] Ahn, Jeong, Kim, *Micromachines* **2019**, *10*, 508.
- [47] N. A. Kulikova, I. V. Perminova, *Molecules* **2021**, *26*, 2706.
- [48] A. Hrynyshyn, M. Simões, A. Borges, *Antibiotics* **2022**, *11*, 69.
- [49] I. Negut, B. Bita, A. Groza, *Polymers* **2022**, *14*, 1611.
- [50] S. E. Yu, S. Chung, H.-S. Ha, D.-H. Kim, S. Baek, T. Y. Kim, S. Lee, H.-J. Yoon, S. W. Chung, J. B. Lee, Y. M. Shin, H.-S. Kim, S. Y. Kim, J.-S. Park, C.-S. Kim, H.-J. Sung, *Adv. Funct. Mater.* **2022**, *32*, 2110368.
- [51] K. M. Aw Yong, Y. Zeng, D. Vindevich, J. M. Phillip, P.-H. Wu, D. Wirtz, R. H. Getzenberg, *J. Cell. Physiol.* **2014**, *229*, 362.
- [52] T. Y. Kim, D.-H. Kim, J.-K. Yoon, S. Kim, S. W. Yi, W. T. Oh, J. Y. Park, H.-S. Kim, M.-L. Kang, J. B. Lee, H.-J. Sung, *Advanced Therapeutics* **2020**, *3*, 2000039.
- [53] D. Zhang, Q. Chen, W. Zhang, H. Liu, J. Wan, Y. Qian, B. Li, S. Tang, Y. Liu, S. Chen, R. Liu, *Angew. Chem.* **2020**, *132*, 9673.
- [54] H.-J. Yoon, S. Lee, T. Y. Kim, S. E. Yu, H.-S. Kim, Y. S. Chung, S. Chung, S. Park, Y. C. Shin, E. K. Wang, J. Noh, H. J. Kim, C. R. Ku, H. Koh, C.-S. Kim, J.-S. Park, Y. M. Shin, H.-J. Sung, *Bioactive Materials* **2022**, *18*, 433.